2014

High Resolution Bathymetric Lidar Data To Hydraulic - Modelling A Mountain Stream By Bathymetric Lidar Data

Wolfgang Dobler

Frank Steinbacher

Ramona Baran

Markus Aufleger

11th International Conference on Hydroinformatics
HIC 2014,New York City, USA

HIGH RESOLUTION BATHYMETRIC LIDAR DATA AS BASE FOR HYDRAULIC-MODELLING OF A MOUNTAIN STREAM

WOLFGANG DOBLER (1), FRANK STEINBACHER (1), RAMONA BARAN (1),
MARCEL RITTER (1), MARKUS AUFLEGER (2)
(1): AirborneHydroMapping GmbH, Technikerstrasse 21 a, 6020-Innsbruck, Austria
(2): University of Innsbruck, Unit of Hydraulic Engineering, Department of Infrastructure, Technikerstrasse 13, 6020-Innsbruck, Austria

Knowledge about the hydraulics in alpine torrents is relevant to quantify flood risks, to study sediment transport and to assess the water-bodies' ecology. Usually, computational fluid dynamics (CFD) simulations are the preferred tool to calculate velocities, water depths and sediment transport for the discharges of interest, which then serve as a basis for the evaluation of flood risks or ecological conditions. To enable reliable calculations, high-quality terrain data of the riverbeds, riverbanks, and floodplains are required. Typically, digital terrain models (DTMs) of the floodplains reconstructed from airborne light detection and ranging (LiDAR) data are combined with terrestrial surveys of riverbanks and riverbeds. The terrestrial surveys are necessary as the lasers (red wavelength) usually cannot penetrate the water surface into the observed water-bodies. Those surveys are labor intense and can be located in difficultly accessible terrain. Therefore, data of the riverbeds' and riverbanks' geometry is hardly available at such a high resolution and extent that is comparable to the airborne LiDAR based data of the floodplains. In this study a newly available airborne water-penetrating LiDAR system (green wavelength) was used to survey alpine torrents. Detailed and extensive data of riverbeds and riverbanks were acquired. Abundant water points were available from the measurement and are used to reconstruct the water table. Depending on the planarity of the point cloud a downsampling was carried out to derive a CFD-mesh for a Telemac-2D simulation. Finally, a calibration was done based on water surface points stemming from the airborne-laser scanning. The LiDAR data turned out to be a very suitable data source for constructing the computational grids of the riverbed. The CFD results demonstrated the new possibilities to compare measured and simulated water heights.

INTRODUCTION

For water engineering one of the most important aspects of hydraulics deals with representing the topography of rivers, floodplains, estuaries or coastal areas. The hydraulic background of water bodies in terms of 2D- or 3D-modeling is influenced by various factors. Among these factors, differences exist in scale and resolution but those differences need to be considered to derive close-to-reality numerical models. Commonly, flood or wave model applications utilize digital elevation models based on high-quality and high-resolution topographic airborne laser

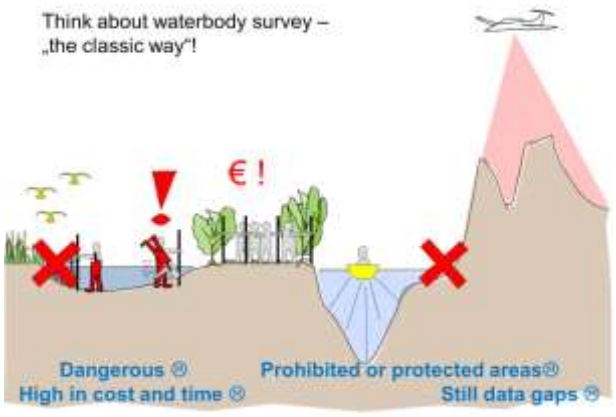

Figure 1. The classic and complex procedure of waterbody and foreland surveying.

data (Figure 1). The digital elevation model of a water body itself is normally represented by simplified and interpolated data based on cross-sections, manually collected during terrestrial fieldwork or by echo sounder data. Due to a lack of spatial and high-resolution water-body information, the modeling of shallow areas like meadows, estuaries, riverbanks or dune structures is highly time consuming, or even impossible (Figure 1). Frequent urban or coastal flooding over the past decades have identified an urgent need to improve and increase our modeling efforts, and to address more explicitly the specific effects of uncertainty in simulations caused by model input data. Society demands reliable and detailed information on magnitude and likelihood of hazardous flood events to design flood mitigation. For this, the assumption of the shape of the water body or manmade protection structures has to be solved and modeling improved by using the actual shape. Furthermore, additional information like surface roughness or the water surface are relevant to calibrate such models. The technology of hydromapping aims to solve this challenge.

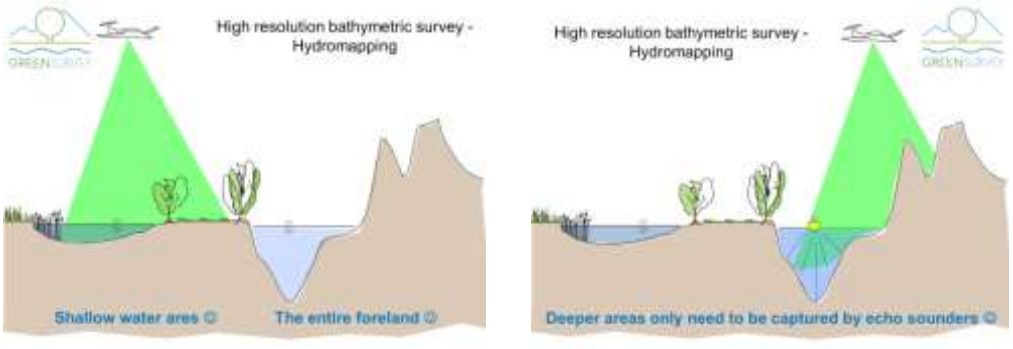

Figure 2. Shallow areas captured by hydromapping, deeper areas captured by echo sounder.

HYDROMAPPING OF THE AHR TORRENT

In this study, a newly available, water-penetrating airborne laser system (green wavelength, FFG research project between the University of Innsbruck and Riegl LMS, Figure 2) was used to survey the alpine Ahr torrent between Sand in Taufers and Bruneck, South Tyrol, Italy, at a length of about 20 km (Figure 3). The survey was performed in December 2012 and took 2 hours in total. The data acquisition by fixed wing aircraft was conducted from an altitude of about 600 m above ground with a pulse repetition rate of 250 kHz and a maximum laser-pulse energy still maintaining eye-safety even for the aided eye. About 33 scan strips have been acquired yielding an average total point density of 20-40 points/m^2.

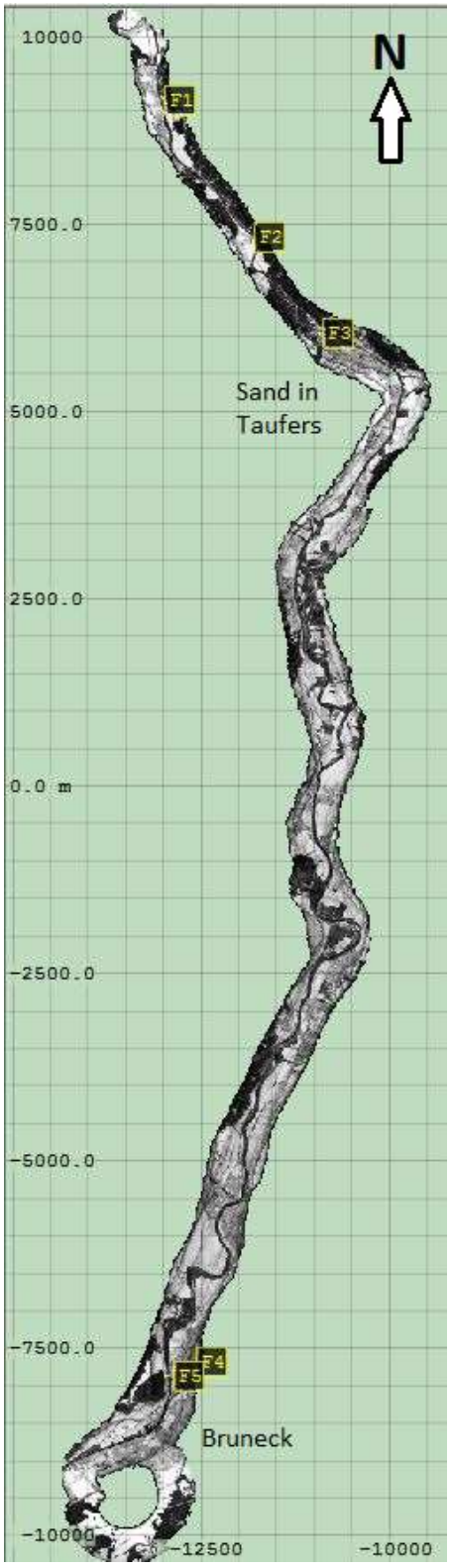

Figure 3. Project area along the Ahr torrent, South Tyrol. Yellow labels depict the reference planes for georeferencing.

Prior to georeferencing of the hydromapping data, the 33 scan strips need to be adjusted to each other in order to derive an internally consistent data set, e.g., no vertical and horizontal offsets among strips. The uncertainty of this adjustment was about 6 cm (standard deviation). The entire point cloud is then georeferenced to UTM 32N coordinates using five terrestrially measured reference planes distributed across the project area in Figure 3. The locations of the reference planes were selected based on the hydromapping data, and the planes were defined by the four outer corners of cross-walks. The uncertainty of the georeferencing process was about 3 cm (standard deviation). Lastly, the point cloud was classified according to **Error! Reference source not found.**, and the correction of the water-depth (refraction) was applied to points located below the actual water-surface level by using the software HydroVISH.

MESH CREATION

For the data evaluation, mesh construction and visualization the software framework **HydroVISH** based on **VISH** (The Vish Visualization Shell; [Benger et al. 2007]) was used. **HydroVISH** allows to combine data from a wide variety of different data sources, observational as well as computational ones. It is a flexible c++ programming environment where data manipulation modules can be added or extended easily. Several modules supporting manipulation, computation and visualization of point clouds are already provided.

The point cloud of the Ahr river consists of $23.1 \cdot 10^6$ points and was classified according to the following properties: ground, vegetation and buildings, river-bed, and water surface illustrated in **Error! Reference source not found.**. The discharge rate (12.12.2012; [South Tyrol 2012]) was 12.00 m^3/s. The part of the river considered for the numerical simulation is approximately 20 km long. The foreland is only partly included in the CFD simulation.

The main task is now to reduce the point density of the point cloud to an appropriate and

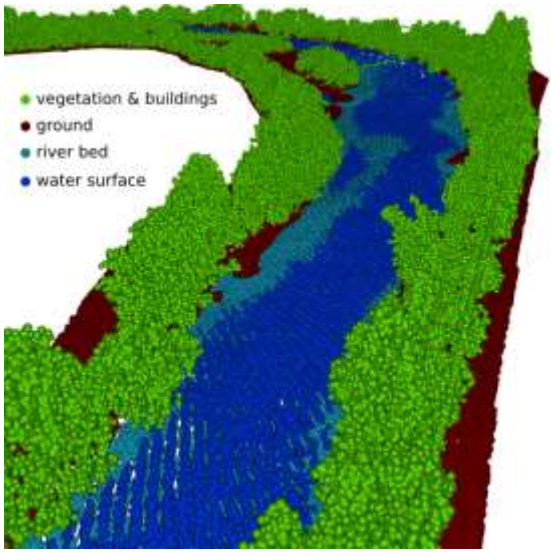

Figure 4: Detailed view of the point cloud of the Ahr river. Colors represent different point classes.

easily-manageable size without losing too many morphological features of the river bed. The first step to derive a 2D-mesh is therefore to use only the ground-, river bed- and bank points (for convenience these points are called "*ground-points*" in the following). Even though the LiDAR-measurements yielded good results along the river bed, there exist some smaller spots where no *ground-points* at all have been gained (Figure 5). This is due to white water effects where the laser beam could not penetrate the water surface, or very dense vegetation is overhanging into the riverbed.

Thus, empty spots in the *ground point* cloud need to be filled up: The first step is to map the point cloud to a uniform grid and use the flood-fill algorithm [Bradski 2008] to mark the cells around the *ground point* cloud as *outside*. The second step is to fill all empty cells which are not marked as *outside* with the mean height value of the neighboring cells (Figure 6). The newly created points (cell-centered) are added to the original *ground point* cloud as is shown in Figure 5.

Figure 5. Red points are artificial points to close holes in the point cloud.

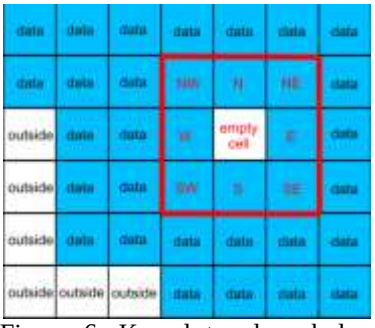

Figure 6. Kernel to close holes. Mean value of the eight directions (N,NE...) are used to fill up the empty cell.

DOWNSAMPLING OF THE POINT CLOUD

Due to the high *ground point* density, a downsampling of the point cloud on a uniform grid has been carried out. In order to capture the majority of morphologic features contained in the point cloud, the downsampling was performed with two different cell sizes: a larger cell size (3 m edge length) for flat areas and a smaller cell size (1.5 m) for non-flat areas. To distinguish if the smaller or the larger grid should be used a "*point distribution tensor*" was calculated, which is defined as [Ritter & Benger 2012]:

$$S(P_i) = \frac{1}{N}\sum_{k=1}^{N} \omega_{ik}(|t_{ik}, r|)\,(t_{ik} \otimes t_{ik}^{\tau}),$$

whereby $\otimes$ denotes the tensor product, τ the transpose and $t_{ik} = P_i - P_k$. The term $\omega_{ik}(|t_{ik}|,r)$ is a weighting function, where r is an user specified distance or radius defining the neighborhood of a point P_i. The weighting function ω_{ik} is zero outside this radius. The distribution tensor is symmetric and positive with three eigen-values. These values are used to classify the tensor via three shape factors [Westin et al. 1997], characterizing the shape of a fitting ellipsoid of the point neighborhood. The three shape factors are:

$$\begin{aligned} c_{linear} &= (\lambda_3 - \lambda_2) \,/\, (\lambda_1 + \lambda_2 + \lambda_3) \\ c_{planar} &= 2\,(\lambda_2 - \lambda_1) \,/\, (\lambda_1 + \lambda_2 + \lambda_3) \\ c_{spherical} &= 3\,\lambda_1 \,/\, (\lambda_1 + \lambda_2 + \lambda_3). \end{aligned}$$

Here, c_{planar} was used to distinguish between flat areas and areas where points are dispersed (Figure 8). Based on a threshold value a grid with two different cell sizes (either edge length 3 m or 1.5 m) is constructed, and the mean height of the corresponding points in the cell are mapped onto the grid (Figure 7).

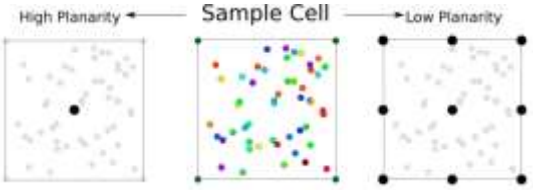

Figure 7. Downsampling of the point cloud: If the planarity of the sample is high all points are replaced by a single point with its mean height, otherwise a subgrid with cell size of 1.5 m is used.

Finally, the downsampled points are triangulated with the **qhull** algorithm [Barber et al. 1996]. A threshold value of $(3^2+3^2)^{0.5}$ for the edge length is used to avoid triangulation outside of the domain (max. cell size of 3 m). The resulting triangulation is shown in Figure 9. This mesh was exported as a SMS-2dm file and imported into BlueKenue (version 3.3.4) for further processing.

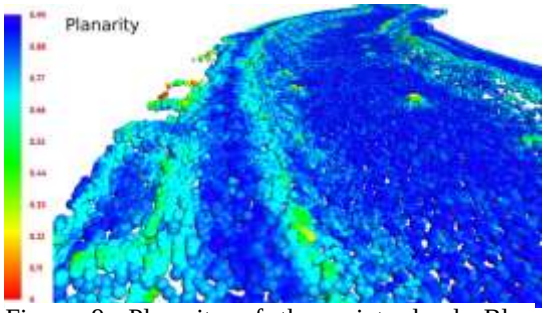

Figure 9. Planarity of the point cloud: Blue denotes high planarity (points are aligned within a plane) and red means no planarity.

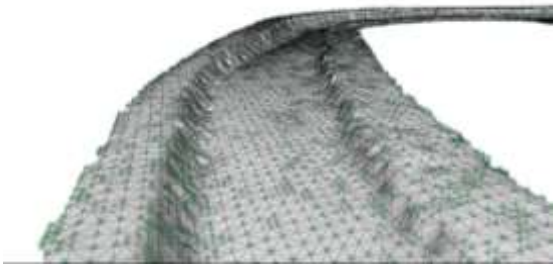

Figure 8. Triangulation of the downsampled point cloud.

CALIBRATION OF THE TELEMAC 2D-SIMULATION

The CFD-simulation was carried out with the open-source software Telemac-2D (version 6.2). The boundary conditions were set in BlueKenue with an inlet-outlet discharge rate of Q = 12.00 m^3/s and corresponding water-level heights derived from the LiDAR-measurement. The mesh-dependency was checked with a 20% coarser mesh-size, and for the turbulence model the k-ε and constant eddy viscosity were tested; the comparison showed no significant differences. For the final calibration-run the constant eddy viscosity was chosen to be 0.1 m^2/s. The values for the friction coefficient (Strickler-values) were automatically calculated by comparing

the instantaneous water height from the CFD calculation with the *target height* of the hydromapping water surface. If the CFD water height was greater than the *target height* from the LiDAR- measurement, the roughness value was changed to a smoother value and vice versa. This procedure was carried out for every hour of physical run-time, and the corresponding roughness value-change was no more than 5%. An upper and lower limit for the roughness of 100 and 10 $m^{1/3}/s$ were used, respectively. If the current water surface was within a range of ± 2 cm of the *target height* no further roughness changes were applied. After 20 hours of physical time the simulation reached a steady-state condition with constant values for in- and outlet discharge, water heights and roughness values. The algorithm for the roughness correction was written in Fortran (the subroutine *corstr.f* provided by Telemac-2D was altered for that purpose), and linked with the executable binary of Telemac-2D.

For the *target water-level height* taken from the LiDAR-measurement a new uniform grid was calculated. The reason for this is shown in Figure 10. The LiDAR points belonging to the water surface had been extracted within a band of 20 cm. These points are split up into cells of 3 x 3 m. Only the uppermost points (99% quantile) are valid water surface points [Mandlburger et al. 2013] and therefore, all water surface points are replaced by a new single point with cell centered coordinates and z = $q_{0.99}$. The newly created uniform grid needs again to be resampled on a denser grid (cell size of 1 m), and is expanded towards the river banks. For water depths lower than 30 cm (Figure 11) no water surface points can be measured by the laser device and therefore an algorithm, similar as shown in Figure 6, is used to expand the water surface toward the river banks. The resulting water surface (green and red points in Figure 11) is mapped to the original CFD-mesh to derive a second mesh for comparing the actual CFD-water height and the *target water height* at each node during the numerical simulation.

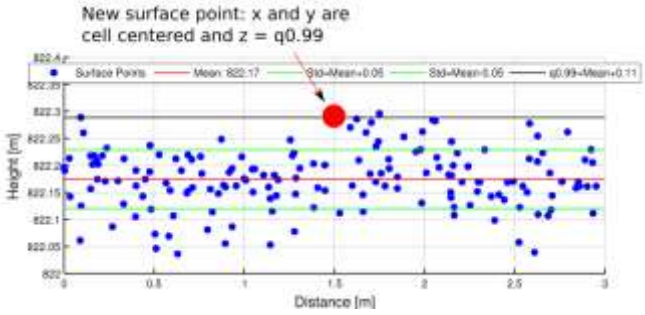

Figure 10. Water surface points within an example cell of 3 x 3 m: Points were mapped on a uniform grid (cell centered). The offset from the mean value is $q_{0.99}$ = 11 cm for this example cell.

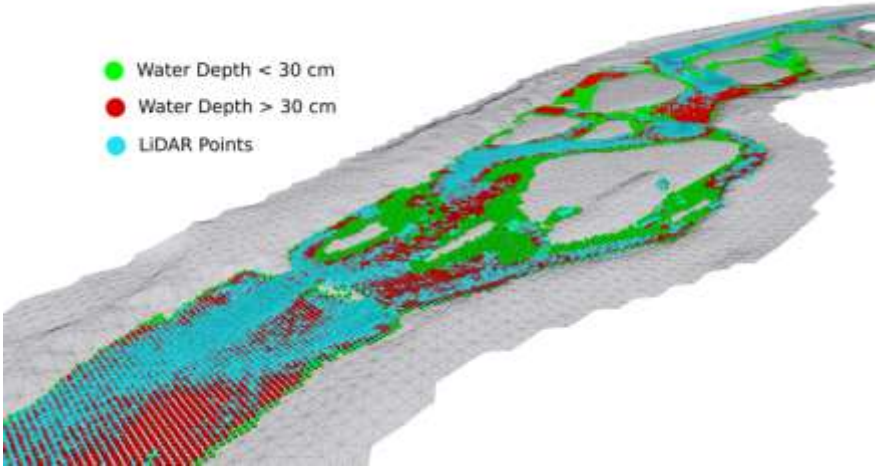

Figure 11. Reconstructed water surface.

The results for the automatically estimated Strickler-values are shown in Figure 12. The mean value for the roughness of the entire wetted area is 35 $m^{1/3}/s$. The difference between the LiDAR and CFD-water surfaces is shown in Figure 13. The mean difference is 8 cm with a standard deviation of 12 cm. This is in good agreement with the accuracy of the strip adjustment of 6 cm.

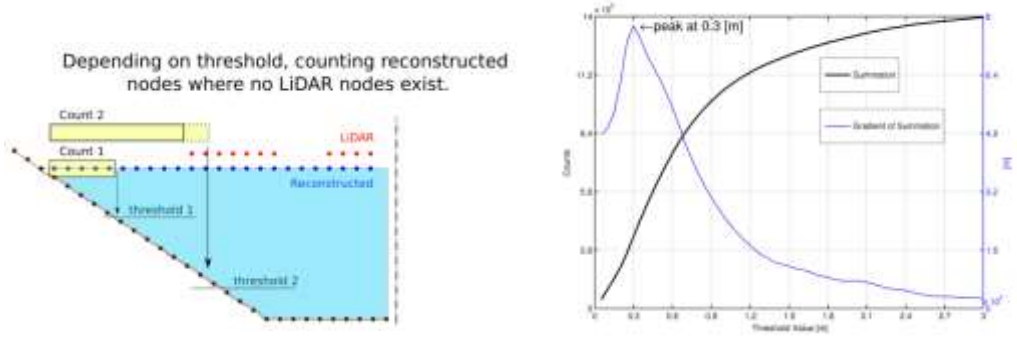

Figure 11. Left Image: Sketch of the calculation of the threshold value. The LiDAR points are mapped on the same uniform grid as the reconstructed water surface points. All points of the reconstructed water surface which have a smaller water depth than the threshold value are summed up only if there exist no corresponding LiDAR points. At a threshold of 30 cm a significant drop of the gradient of the summation can be seen (right figure).

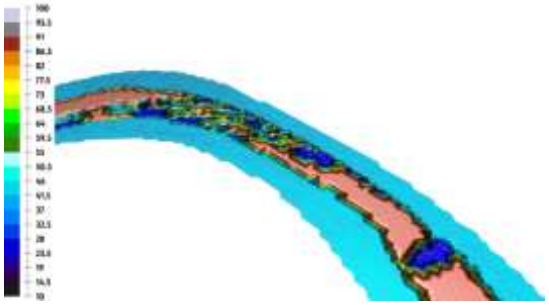

Figure 12. Detailed view of the calculated roughness (Strickler Value, $m^{1/3}/s$).

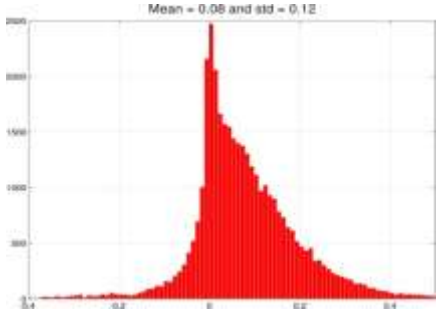

Figure 13. Histogram of the height difference between CFD- and LiDAR water surface.

CONCLUSIONS

The high-resolution LiDAR-data with an accuracy of approximately 6 cm (relative accuracy derived from the strip adjustment) are very suitable for a numerical simulation. To reduce the amount of information of the point cloud a downsampling on a uniform grid with two different cell sizes has been carried out. In order to switch between the larger and smaller cell sizes of the uniform grid a point distribution tensor was calculated; if the points are aligned within a plane (high planarity) the larger cell size is used, otherwise the smaller one (low planarity). The downsampled point cloud can be easily triangulated by a **qhull** algorithm and exported as a 2DM (SMS) mesh for further boundary treatment in BlueKenue.

The calibration of the CFD simulation was performed by using the water surface points of the airborne-laser scanning. Further treatment of these points is necessary due to the fact that

the exact water surface needs to be calculated out of a measured water surface band of about 20 cm. Therefore, only the topmost water surface points (99% quantile) are used to create an additional *target water-height* mesh. The calibration was finally done by comparing the *target height* with the heights of the resulting numerical simulation at every hour of physical run-time; if the heights at each node were not equal, the roughness parameter was slightly changed to lift or reduce the water surface height. For water depths smaller 30 cm, no LiDAR water surface points can be measured with the laser device, and thus the *target height* was expanded toward the river banks to cover the entire water surface of the Ahr river. The results of the comparison between the *target height* and the height calculated by Telemac-2D showed acceptable agreement, where the mean difference is 8 cm and the standard deviation 12 cm with water depths in the range of 0.15 to 2.5 m. A future task is to control the measured water surface of the green laser device with terrestrial measurements of the actual water table. The comparison between the red and green laser used to measure the water surface yielded already promising results [Mandlburger et al. 2013].

REFERENCES

Barber C.B., Dobkin D.P. and Huhdanpaa H.T., The Quickhull algorithm for convex hulls. ACM Trans. on Mathematical Software, 22 (1996), p. 469–483. Available at: http://dx.doi.org/10.1145/235815.235821.

Benger W., Ritter G. and Heinzl R., The Concepts of VISH. In 4. High-End Visualization Workshop, Obergurgl, Tyrol, Austria, June 18-21, 2007. Berlin, Lehmanns Media-LOB.de, p. 26–39.

Bradski A., Learning OpenCV, [Computer Vision with OpenCV Library ; software that sees] 1. ed., O`Reilly Media (2008).

Mandlburger G., Pfennigbauer M. and Pfeifer N., Analyzing near water surface penetration in laser bathymetry - A case study at the River Pielach. In ISPRS Annals of the Photogrammetry, Remote Sensing and Spatial Information Sciences, (2013) p. 175–180. Available at: http://publik.tuwien.ac.at/files/PubDat_221149.pdf.

Ritter M. and Benger W., Reconstructing Power Cables From LIDAR Data Using Eigenvector Streamlines of the Point Distribution Tensor Field. In Journal of WSCG Vol 20., No.3, p. 71+, 20th International Conference in Central Europe on Computer Graphics, Visualization and Computer Vision (2012), Plzen, Czech Republic.

South Tyrol, Province of Bolzano, Gage height and Discharge rate (2012), Available at: http://www.provinz.bz.it/.

Westin C., Peled S., Gudbjartsson H., Kikinis R. and F. Jolesz, Geometrical diffusion measures for mri from tensor basis analysis. In Proceedings of ISMRM, Fifth Meeting (1997), Vancouver, Canada.